PROCEEDINGS, 44th Workshop on Geothermal Reservoir Engineering
Stanford University, Stanford, California, February 11-13, 2019
SGP-TR-214

Structural and Paleomagnetic Analysis of Geothermal Drill Core, Akutan Alaska

Molly Johnson, Pete Stelling

Environmental Studies Building 240, 516 High St, Bellingham, WA 98225

johns877@wwu.edu, stellip@wwu.edu

Keywords: Paleomagnetics, core reorientation, geothermal

ABSTRACT

Hot Springs Bay Valley (HSBV) geothermal resource area on Akutan Island, Alaska, has increased fluid output and temperature by almost a magnitude, between 1981 and 2012 (Bergfeld et al., 2014). These increases have been attributed to increased permeability along NW-SE trending faults that may have been activated during a seismic swarm in 1996. In 2010 two unoriented drill cores were collected in Hot Springs Bay geothermal resource area. In this study we reorient sections from one the highly fractured core with paleomagnetics to test this model of geothermal reservoir evolution at Akutan. The core is composed of interlayered island arc volcanics and shallow marine mudstones. Paleomagnetic plug samples were drilled from the volcanics. Continuous sections of the core were reoriented using the declination of the remanent magnetization (RM) as an indication of geographic north. Structure from motion software was used to create digital reconstructions of the core from photographs. The resulting models were then flattened with a cylindrical projection into a 2D depiction of the outside of the core. The orientation of veins and the relationship between vein sets were measured from these projections. Results show that NNW trending, ENE dipping veins dominate the system and show evidence of sustained fluid flow, whereas veins of other orientations show single event fluid flow. Further, preliminary cross-cutting relationships suggest earlier fluid flow was primarily hosted by N-trending, E-dipping fractures and that more recent activity has shifted some of this fluid flow to SE-trending, SW-dipping structures. These younger structures are parallel to surface ruptures observed from the 1996 seismic swarm. This supports the hypothesis of Bergfeld, et al., (2014) that rupture along a SE trending fault during the 1996 seismic swarm contributed to the permeability of the system.

1. INTRODUCTION

The City of Akutan and adjacent Trident Seafoods processing plant on Akutan Island (Figure 1B) would greatly benefit from a local source of clean energy. The City of Akutan and Trident Seafood's current energy needs are being met by burning 4.3 million gallons of imported diesel fuel annually (Kolker et al., 2011). In 2018 residential electricity rates in Akutan were 0.3117 $/kWh; 162% greater than the national average. The need here could be met by establishing a geothermal power plant in Hot Springs Bay Valley (HSBV) geothermal resource area, which would add valuable infrastructure to the island, help the community to become more energy independent, and diversify the job market

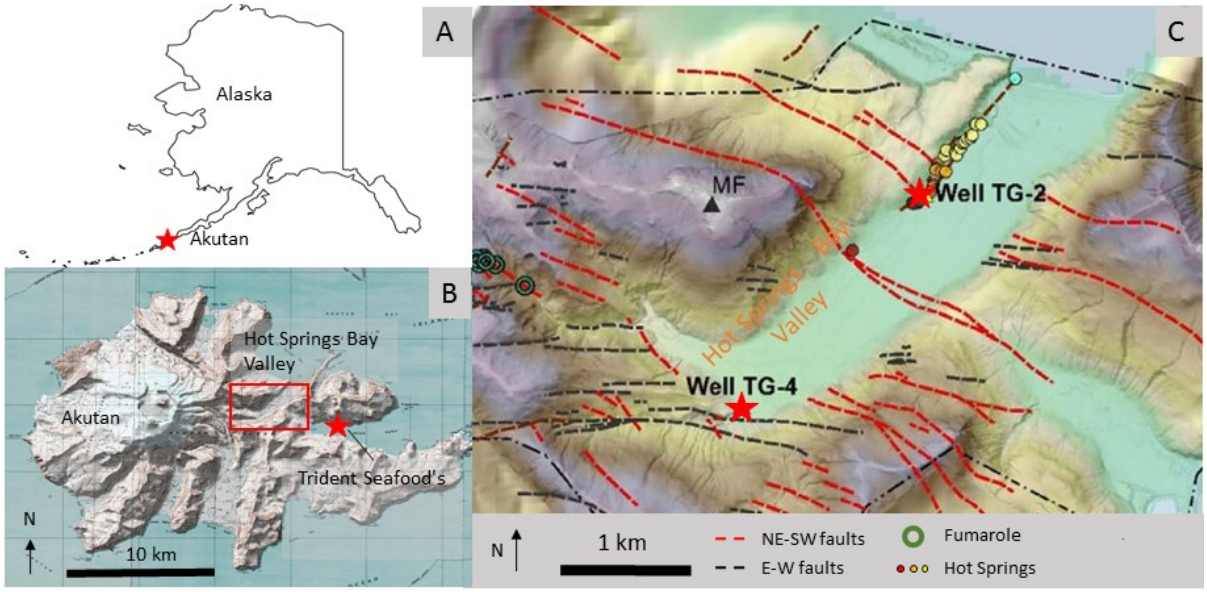

Figure 1: Map of A) Akutan in relation to Alaska denoted by the red star; B) the location of hot springs bay valley (HSBV), on Akutan Island (red box) and Trident Seafoods processing plant (red star); C) the location of well TG-4 and structural and geothermal features within HSBV. MF = Mt. Formidable. Modified from Stelling et al. 2015.

The Aleutian Island chain, and Akutan Island in particular (Figure 1A), has high potential for geothermal power production (Motyka et al., 1993; Kolker et al., 2012; Stelling et al., 2015). Previous geochemical studies (Bergfeld et al., 2014; Stelling et al., 2015) and down whole measurements of two slim wells (Kolker et al., 2011) have confirmed enough reservoir heat to produce 2-3 MWe from the resource (Stelling et al., 2015). Furthermore, Bergfeld et al., (2014) noted an 134% increase in discharge of the thermal creek and increased temperatures resulting in a 29MW thermal output for the hot springs, which is about a magnitude greater than previous studies (Motyka et al., 1988). These increases reflect both an increase in heat and an increase in permeability of the system between the early 1980's and 2012. Bergfeld et al., (2014) postulated that rupture of the NW-SE striking fault during the seismic swarm in 1996 could explain the increased permeability and notes the longevity of the increased heat output, if their hypothesis is indeed correct. The primary goal of this project is to determine the orientation of permeable fractures in the subsurface of the HSBV geothermal resource, and therefore test Bergfeld's hypothesis.

Both wells were recovered entirely as unoriented core, with variable degrees of fracturing. Well TG-2 is 254 m (833 ft.) deep, located on the northern side of the lower valley close to the eastern extent of the hot springs (Figure1C). Approximately 90% of the TG-2 core was recovered. Well TG-4 is 457.2 m (1500 ft.) deep and located along the southwestern valley wall at the confluence of the upper and lower valleys (Kolker et al., 2011), with core recovery of ~98% (Figure 1C). Reorientation of segments from TG-4 was done using the declination of RM in the core as an indicator of geographic north. Using RM is an inexpensive and proven technique for orienting already-drilled core in petroleum exploration (Fuller, 1969; Allerton et al., 1995; Hailwood and Ding, 1995). This technique is challenging in hydrothermal systems because high temperature fluids circulating through the fractures can provide enough heat to reset or overprint the primary magnetic signal in the surrounding country rock. Additionally, the high latitude of Akutan means that the inclination of the magnetic signal is very steep (72° in the modern field), and therefore the declination signal has a high degree on intrinsic error. Furthermore, the magnetic signal could have been overprinted by the actual drilling of the core (Hailwood and Ding, 1995). For these reasons, and others discussed below, only two segments, between 942-983 ft. depth and 1030-1066 ft. depth in TG-4 have been reoriented and the fractures measured for this study.

2. GEOLOGIC CONTEXT

Akutan Island is one of the easternmost Aleutian Islands, which represents the volcanic arc formed from the northwestward subduction of the Pacific plate under the North American plate. The active volcano dominates the western half of the island. The eastern half of the island is composed of glacially scoured remnants of ancient volcanic activity. Romick et al., (1990) separated the rock units on Akutan into three broad categories. The oldest rocks on the island are the hot springs volcanics (HSV), overlain by the ancestral Akutan volcanics (AKV), and the modern Akutan volcanics (MOD) with the most recent lava flows in the north of the island. The AKV and MOD are separated by an angular unconformity (Romick et al., 1990). The AKV are cut by dikes of MOD which mostly parallel the ridges that extend out from Akutan volcano (Byers and Barth, 1953). Akutan has been the most active volcano in the region for decades (Finch, 1935; Miller et al., 1998). Historical records show that major activity on the volcano occurs approximately every 20 years (Byers and Barth, 1953), the most recent of which was a seismic swarm in 1996, which has been attributed to the emplacement of a shallow dike (Lu et al., 2005). Surface mapping shows three orientations of structural features on Akutan Island (Stelling et al. 2015, Richter et al. 1998). These are fault scarps, fractures, dikes and lineaments that are oriented WNW-ESE, NE-SW, and E-W (Figure 1C). There are two geothermal systems on Akutan (Motyka et al., 1993), one in the summit crater and one on the flank of the volcano in HSBV.

The seismic swarm of 1996 consisted of >3000 earthquakes (M_{max}=5.1) that reactivated WNW-ESE striking faults south of HSBV and across the island (Lu et al., 2005). The change in ground surface morphology before and after the seismic activity is consistent with the emplacement of a dike with its shallowest depth at 0.4 km beneath the northwest flank of Akutan volcano oriented parallel to the WNW striking ground cracks (Lu et al., 2005). The documented subsidence on the south-east flank could be explained by depressurization of the hydrothermal field facilitated by movement along normal faults. Subsidence of the northwest flank in 1996-1997 by about 20mm is most likely due to the cooling and degassing of the intrusion (Lu et al., 2005).

HSBV is a glacially carved valleys on the northeastern side of island, which consists of two valleys. The upper valley, oriented NW-SE and the lower valley, oriented NE-SW. The two valleys meet in the southwest, forming an approximately 90° bend in the valley (Figure 1C) suggesting that the glacier's path may have been structurally controlled. A prominent NW-SE striking normal fault cuts through HSBV and has a down-to-the-south slip direction (Richter et al. 1998). Most faults mapped in HSBV have dips to the south and show a down-to-the-south dip slip or oblique slip motion with dip angles between 50° and near vertical, however nearly a third of the faults mapped throughout the island do not have dip direction constrained. Fracture traces also dip between 50° and near vertical, but the dip direction is bimodal to the north and south (Stelling et al., 2015).

The HSBV hydrothermal system hosts a fumarole field at the head of the upper valley and a string of hot springs extending ~1 mile along the northern wall of the lower valley (Finch, 1935; Motyka et al., 1993; Symonds et al., 2003; Kolker et al., 2012; Bergfeld et al., 2014; Stelling et al., 2015). The fumaroles and the hot springs are likely connected and stem from the same deep reservoir. The current conceptual model by (Stelling et al., 2015) is based on gas geochemistry, silica and cation geothermometry, geophysics and down-hole temperature measurements. According to this model there is a high temperature upflow under the flank fumaroles that bifurcates into a lower temperature outflow daylighting at the hot springs. Kolker et al. (2012) proposed two different flow paths for the outflow, one following HSBV to the south, and the other curving north under Mt. Formidable just north of the main section of HSBV (Figure 1C). A geochemical study of the hot springs (Bergfeld et al., 2014) reported a heat output of ~29MW, which is about an order of magnitude higher than studies done in the 1980's (Motyka et al., 1993). Bergfeld et al. (2014) suggest this increase in heat and discharge is the result of increased fracture density and dilation along the WNW-ESE oriented normal fault between the hot springs and the fumaroles that was re-activated during the 1996 seismic swarm.

The cores consist of interbedded basalt and andesite lavas, andesitic and dacitic tuffs, and mass wasting deposits. Similarities between lithologic units and variable alteration have made traditional stratigraphy unsuccessful. The hydrothermal alteration can take the form of high-density hairline veining, mottled white and green mineralization in the matrix of mass wasting deposits, or pale green mineralization around fracture planes and lithologic contacts that extend several centimeters into the rock. Areas of high permeability are often associated with the brecciated tops of vesicular basalt and andesite flows or with hydrothermally altered and fractured tuffs (Kolker et al., 2011).

3. METHODS

3.1 Paleomagnetism

The fractured core pieces were reassembled into "runs" using the fit of individual pieces or through going rock fabric, and a reference mark (N') was made along the length of each section (Figure 2). For this study runs from 943-983 ft. depth, and 1030-1066 ft. depth in well TG-4 were analyzed. These runs were chosen because they are the longest and contain the highest density of fractures and cross cutting veins. Sampling for RM analysis was restricted to igneous units; basalts, andesite, and tuffs that were relatively free of veining and at least two feet away from intense hydrothermal alteration. Which occurs mostly along contacts between lithologies or the brecciated tops of flows. Samples are grouped in a hierarchy by locality, site, sample, and specimen. Each core is a locality, each run in the core is a site, each unit flow in that run is sampled, and each individual plug sample is a specimen with the naming scheme: (footage)-(piece number in the box)(specimen in sample). All analysis was done in the Pacific Northwest Paleomagnetics Laboratory following standard demagnetization procedures. The goal being to isolate the original chemical remanent magnetization (ChRM) from the time of crystallization. Six specimens were drilled in each run that hosted an appropriate lithology. If the run had multiple flows appropriate for sampling, three specimens were taken from each additional flow. Samples were drilled relative to the false north mark through the center of the core, so that the positive x direction on each specimen is parallel to N' and in the up-core direction (Figure 2). The plug samples are taken from the center of the core to avoid drill induced remagnetization that could have affected the outside of the core (Pinto and McWilliams, 1990). Half of the specimens from the samples with six specimens and all the specimens from the additional samples were demagnetized with increasing strength of an alternating field in the D-Tech 2000 AF (de)magnetizer. The other half of the six specimen samples were thermally demagnetized. Specimens with high magnetic moments were measured on the spinner magnetometer and the rest were measured on the 3-axis 2-G Enterprises model 755 cryogenic magnetometer between each demagnetizing step. Principle Component Analysis (PCA) (Kirschvink, 1980) was used to define paleomagnetic directions from demagnetization steps within the PuffinPlot (Lurcock and Wilson, 2012) software. Fisher statistics (Fisher Ronald Aylmer, 1953) were used to calculate the mean declination and inclination of selected specimens. Finally, directions with negative inclinations were converted to the lower hemisphere so that the declination direction is pointing to the north rather than the south.

Because Akutan is at a high latitude the inclination angle is steep and therefore there is inherent error in the declination direction of any magnetic signal. Also because of the limited usable sample sites there is not enough time sampled to average out paleo secular variation. These two factors compounded produce and error of around 30° in the declination direction for each run individually. Therefore, vein set orientations and their implications must be discussed generally. For example, this study has not provided the resolution to distinguish between an NNE trending vein set and a NE trending vein set, although the relationship between fracture sets within a single run are accurate and precise.

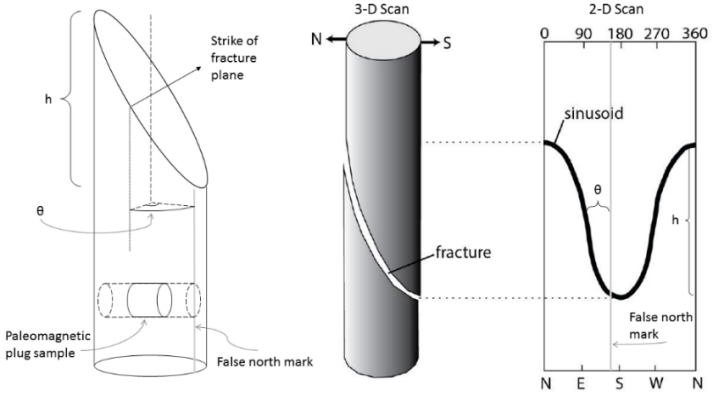

Figure 2: Cartoon showing the position of plug samples for paleomagnetic analysis relative to the false north mark (N'), and a representation of fractures in the 3-D and "unrolled" 2-D states. The height (h) of the sinusoid and the distance from N' (Ɵ) are used to calculate the strike and dip of the fracture or vein from the 2-D scans. The reorientation factor is the difference between the false north mark and true north measured with paleomagnetics.

3.2 Structure from Motion.

Each selected core run was photographed with a Nikon COOLPIX B500 digital camera. The core segments were placed on a rack with a green screen background, which was masked out of the images. Model building followed the standard Agisoft workflow, and a cylindrical projection was used to create an "unrolled" image of the outside of the core (Figure 2). ImageJ was used to generate a list of pixel

coordinates from these images from which the strike, dip, and depth of fractures, veins, contacts and matrix permeability were calculated in an excel spread sheet. The mineral fill was identified, and rake of slicken lines measured by hand. Cross cutting relationships were noted if present. A vein was deemed "cross cutting" where there were subtle offsets or where the mineralization clearly overprinted the other structure. If a fracture or vein was offset by more than a few millimeters it was not measured, as the offset h measurement would not produce and accurate dip data.

4. RESULTS

4.1 Paleomagnetic Reorientation

Paleomagnetic directions throughout each run varied between samples and sometimes between specimens within the sample. This was to be expected given the multitude of possible overprinting causes (i.e. drilling, hydrothermal fluid, dike intrusion etc.). Signals that were deemed legitimate were consistent over multiple specimens and samples, had a reasonable geologic interpretation, and a normal or reverse inclination between ~65º and 85º. The reasonable geologic interpretation also included having at least 2, but preferably 3 components. Because if the first one, and or second components could be explained by an overprint then the last one is likely the original signal, as the weaker signals are removed first in the demagnetization process. Or put another way: if the signal only had one component there was no way of telling weather or not it was due to remagnetization or if it was the original signal. Directions with an inclination greater than 85º do not have reliable declination directions and therefore were not used for reorientation. Signals that passed all these tests were used to reorient the structural data in the corresponding runs. Results are presented in Table 1. Each run has a ±30º error that is inherited from the paleomagnetic data, which is shown in the following figures as an error bar extending from the center of clustered orientations.

Table 1: Results of demagnetization for runs 942-983 ft. and 1030-1066 ft. depth in core TG4. Cryo= cryogenic magnetometer. Max T= maximum temperature (Cº) reached in thermo-demagnetization. Max Field= maximum magnetic field (mT) reached in alternating field demagnetization. In observation and interpretation columns I= inclination and D= declination. A (-) mark in the Chosen vector columns indicates no vector was used from that sample. The maximum angular deviation (MAD3) angle is a measure how well the data points are aligned in a vector, with smaller angles indicating less spread in the data.

Site (Run)	Sample (Lithology)	Specimen	Demagnetization method	Magnet-ometer	Max T	Max Field	Number of components	Observations	Interpretation	Chosen Vector		MAD3
										Inclination	Declination	
942-983	Andesite	947-10A	Alternating Field	Cryo		60	2	Inclination is lower than 60°	Sequence no longer in original position	-	-	-
		947-10B	Alternating Field	Cryo		70	2			-	-	-
		947-10C	Alternating Field	Cryo		70	2			-	-	-
	Andesite	955-9A	Alternating Field	Cryo		70	1	Alternating D between specimens	Sampling overprint	-	-	-
		955.5-11A	Alternating Field	Cryo		70	1			-	-	-
		955.5-11B	Alternating Field	Cryo		70	1			-	-	-
	Basalt	957-15A	Alternating Field	Spinner		35	2	Vertical 1st component, inconsistant 2nd component	Drill string overprint	-	-	-
		957-15B	Alternating Field	Cryo		40	2			-	-	-
		957-15C	Alternating Field	Cryo		40	2			-	-	-
	Andesite	965.5-11A	Thermo	Cryo	395		2	1st component is consistent with 2nd component in 971-2. 2nd component has I >85°	Basalt at 971 intruded and overprinted Andesite	73.03	248.45	1.67
		965.5-11B	Alternating Field	Cryo		35	2			82.44	209.03	1.69
		965.5-11C	Thermo	Cryo	420		2			71.86	247.82	5.24
		965.5-11D	Alternating Field	Cryo		30	1			-	-	-
		965.5-11E	Thermo	Cryo	449		2			69.46	234.93	5.47
		965.5-11F	Alternating Field	Cryo		30	2			79.59	214.89	2.73
	Basalt	971-2A	Alternating Field	Spinner		20	2	Slight change in D between 1st and 2nd components. I between 64° and 75°	2nd component is original ChRM	75.91	186.83	0.74
		971-2B	Alternating Field	Cryo		50	2			69.54	207.82	4.52
		971-2C	Alternating Field	Spinner		35	2			64.1	212.88	2.24
1030-1066	Basalt	1041-16A	Thermo	Cryo	500		3	1st and 2nd component has I similar to modern I and varied D. 3rd component is Reverse between -53° and -64°	1st and 2nd components are sampling and or drilling overprint. 3rd component is original ChRM	-64.67	200.39	1.93
		1041-16B	Alternating Field	Cryo		15	1			-	-	-
		1041-16C	Thermo	Cryo	390		3			-53.07	207.69	4.73
		1041-16D	Alternating Field	Cryo		15	1			-	-	-
		1041-16E	Thermo	Cryo	500		2			-	-	-
		1041-16F	Alternating Field	Cryo		15	1			-	-	-
	Gabbro	1042-1A	Alternating Field	Cryo		40	2	1st component has I similar to modern. 2nd component is -61° and -76°	1st component is drillstring overprint 2nd is ChRM	-61.48	210.22	4.66
		1042-1B	Alternating Field	Cryo		40	2			-75.92	211.83	2.88
		1042-1C	Alternating Field	Cryo		40	2			-72.98	214.96	3.72
	Andesite	1053-4A	Alternating Field	Cryo		40	2	1st and 2nd are almost indistinguishable	could be drilling overprint or ChRM	-	-	-
		1053-4B	Alternating Field	Spinner		50	2			-	-	-
	Andesite	1064-4A	Alternating Field	Spinner		50	2	I is near vertical	Drill string overprint	-	-	-
		1064-4B	Alternating Field	Spinner		30	2			-	-	-
		1064-4C	Alternating Field	Spinner		30	2			-	-	-
	Basalt	1065-16A	Alternating Field	Spinner		30	2	1st component is vertical, 2nd is consistant with 2nd component at 1053	1st is drilling overprint 2nd could be ChRM	-	-	-
		1065-16B	Alternating Field	Spinner		30	2			-	-	-
		1065-16C	Alternating Field	Spinner		25	2			-	-	-

In the 942-983 ft. run there is a clear and consistent direction with a reasonable geologic explanation (Table 1, observation and interpretation columns). The interpretation is that the basalt at 971 ft. depth intruded and the heat caused a thermal overprint in the andesite flow directly above it (sample 965-11). The evidence for this is that the first component in the andesite, the overprint, aligns well with the second component, the original ChRM, in the basalts. See Table 2.

Table 2: Inclination and declination (in °) of site means calculated by fisher statistics. Alpha95 is the radius (in °) of 95% confidence. The precision parameter (k) is a measure of dispersion with higher values indicating more tightly clustered directions.

Run	Inclination	Declination	Lower Hemisphere Corrected		Alph95 of site	k of site
			Inclination	Declination		
942-983	74.2	221.9	--	--	5.8	92.8
1030-1066	-65.7	208	65.7	28	8.9	74.3

In run 1030-1066 there are two reasonable directions that could be the ChRM. The signal that is consistent between samples 1041-16 and 1042-1 has a reverse inclination, which means that it is definitely not a drill string overprint. These samples also have a first or second component with normal polarity that are consistent in inclination but vary in declination. This is interpreted as an overprint caused by drilling. The signal that is consistent between sample 1053-4 and 1065-16 has a very low MAD3 angle (which means that it is well clustered), an inclination that matches the modern inclination is at Akutan, and a consistent declination. This could be the original ChRM, a modern overprint from hydrothermal fluids, or a drill string overprint. Sample 1065-16 has a first component that is horizontal, something that is common throughout the core which we have interpreted as a sampling overprint because the specimens where drilled horizontally from the core (Figure 2). There is enough uncertainty in the origins of the signal from 1053-4 and 1065-16 to justify not using this signal. Additionally, the signal from the 1041-16 and 1042-1 samples is most likely held by magnetite or titanomagnetite, based on the mT and temperature steps that define the signal. Magnetite and titanomagnetite hold magnetic signals very well, therefore the reverse signal in 1030-1066 was used to reorient the core.

4.2 Fracture Sets

Fractures are defined as a break with no mineralization, whereas veins have mineral fill. Fractures have shallow to moderate dips and vary in strike direction. The average is centered around horizontal (Figure 3B). Mineralized veins have dips ranging from ~60° to <10°, with concentrations trending NNW, dipping to the ENE and trending ESE, dipping to the SSW (Figure 3A). The veins in the 1030-1066 ft. run are much more prominent in the NNW-striking direction than in the ENE-striking direction, whereas veins in the 942-983 ft. run approximately equally split between NNW-striking and ENE-striking. The following sections are subsets of the vein orientations.

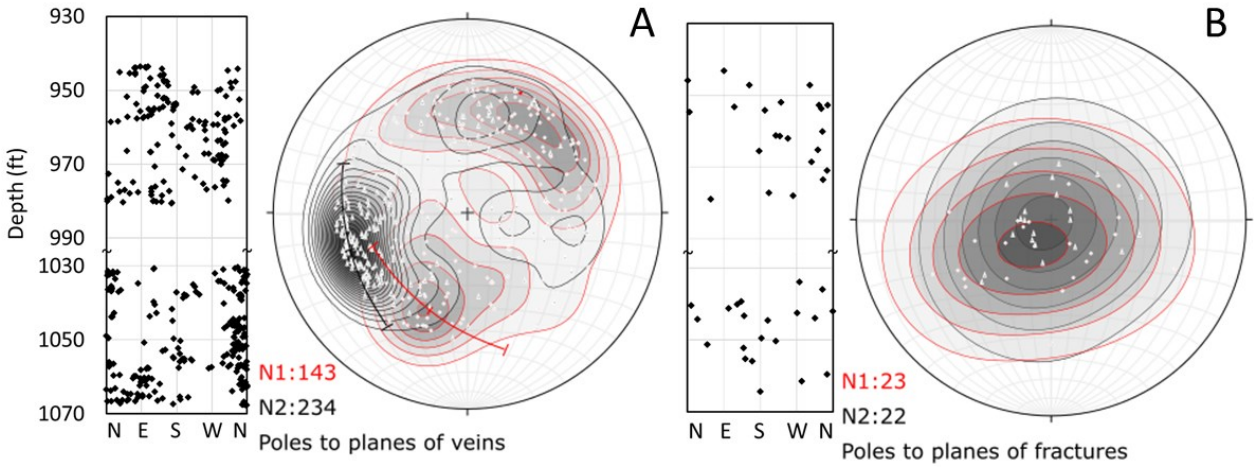

Figure 3: Stereonets of poles to planes for A) mineralized veins and B) non-mineralized fractures. Measurements from the 942-983 ft. run are in red, N1; 1030-1066 ft. run are in black, N2. Kamb contours have a significance level of 3 and an interval of 2. N indicates the number of measurements. Error bars are ±30°. Note the scale break on depth verses strike plots.

4.2.1 Vein Sets Based on Mineralogy

Veins in the core can be separated into three categories based on the vein-filling mineralogy. Veins filled only with calcite (cal) tend to be NW-SE striking with a nearly bimodal dip to the NE and SW, though there are slightly more dipping to the NE (Figure 4A). This trend is consistent between runs, though the dip direction is more evenly split in the 942-983ft. run. Veins filled with hematite (hem) + chlorite (chl) + cal are SSE trending and WSW dipping in the 942-983 ft. run, and N tending and E dipping in the 1030-1066ft. run (Figure 4B). Veins filled with chl + cal are mostly NW-SE trending with a bimodal dip direction in the 942-983 ft. run. In the 1030-1066 ft. run cal and chl filled veins are predominantly NNW trending and ESE dipping though there is a small ESE trending, SSW dipping population.

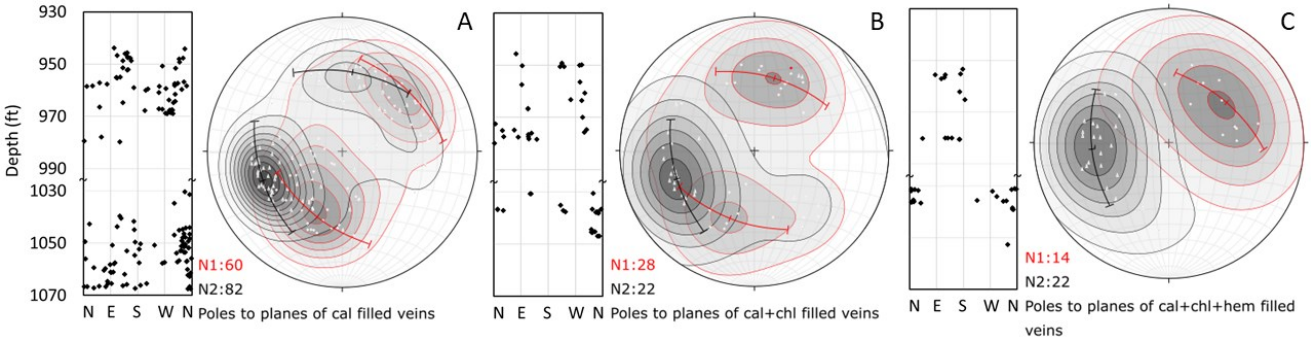

Figure 4: Stereonets of poles to planes for A) calcite filled veins, B) calcite, chlorite, and hematite filled veins, and C) calcite and chlorite filled veins. Measurements from the 942-983 ft. run are in red, N1; 1030-1066 ft. run are in black, N2. N indicates the number of measurements. Kamb contours have a significance level of 3 and an interval of 2. Error bars are ±30°. Note the scale break on depth verses strike plots.

Veins that are laminated and veins that show dip slip extension are split between NNW and ESE-striking in the 1030-1066 ft. run but only SE-trending in the 942-983 ft. run (Figure 5A). Laminated veins are common throughout the 1030-1066 ft. run, and often show at least three generations of mineral growth (Figure 5B), however there is no consistent pattern in the order of mineral growth, for example one vein might have chl in the center with cal on the edges and another vein with a similar orientation and depth will have cal in the center and chl on the edges, or cal on one side chl on the other. Veins that show dip-slip extension are less abundant, but still noteworthy. These are filled only with cal (Figure 5C,D) but are often found near laminated veins as shown in Figure 5B.

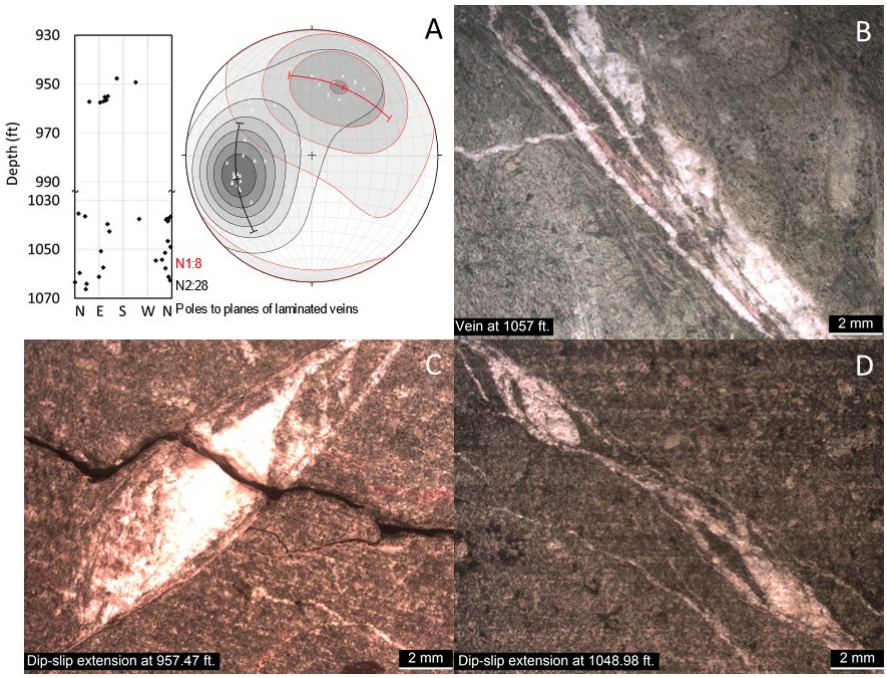

Figure 5: A) Stereonet of poles to planes for laminated veins and veins showing dip slip extension. Measurements from the 942-983 ft. run are in red, N1; 1030-1066 ft. run are in black, N2. N indicates the number of measurements. Kamb contours have a significance level of 3 and an interval of 2. Error bars are ±30°. Note the scale break on the depth verses strike plot. B) Laminated vein of cal (white), hem (red), and chl (dark green) at 1057 ft., and evidence of dip-slip extension at C) 957.47 ft. and D) 1048.98 ft. showing the episodic nature of vein growth.

4.2.2 Vein Sets Based on Width

Most veins are 1mm wide or less. There are veins striking in all directions, though most are NNW trending and NNE dipping (Figure 6A). There is a smaller concentration that is ESE trending and SSW dipping. The strike of the 1mm or less veins is nearly random in the 942-983ft run, whereas it is concentrated in the NNW in the 1030-1066ft. run. Veins that are 2-4mm thick are again mostly SSE trending and WSW dipping in the 942-983 ft. run, but mostly NNW trending and NNE dipping in the 1030-1066 ft. run, with is a small concentration that is SE trending and SW dipping (Figure 6B). Veins that range in width from 5-7mm have trends that are scattered around N with dips to the E, though a very small subset have trends to the S and dip to the W (Figure 6C). The widest veins, >9mm are almost all trending N to NW and dipping to the NE with one exception (Figure 6D). Thick veins are much more common in the 1030-1066 ft. run.

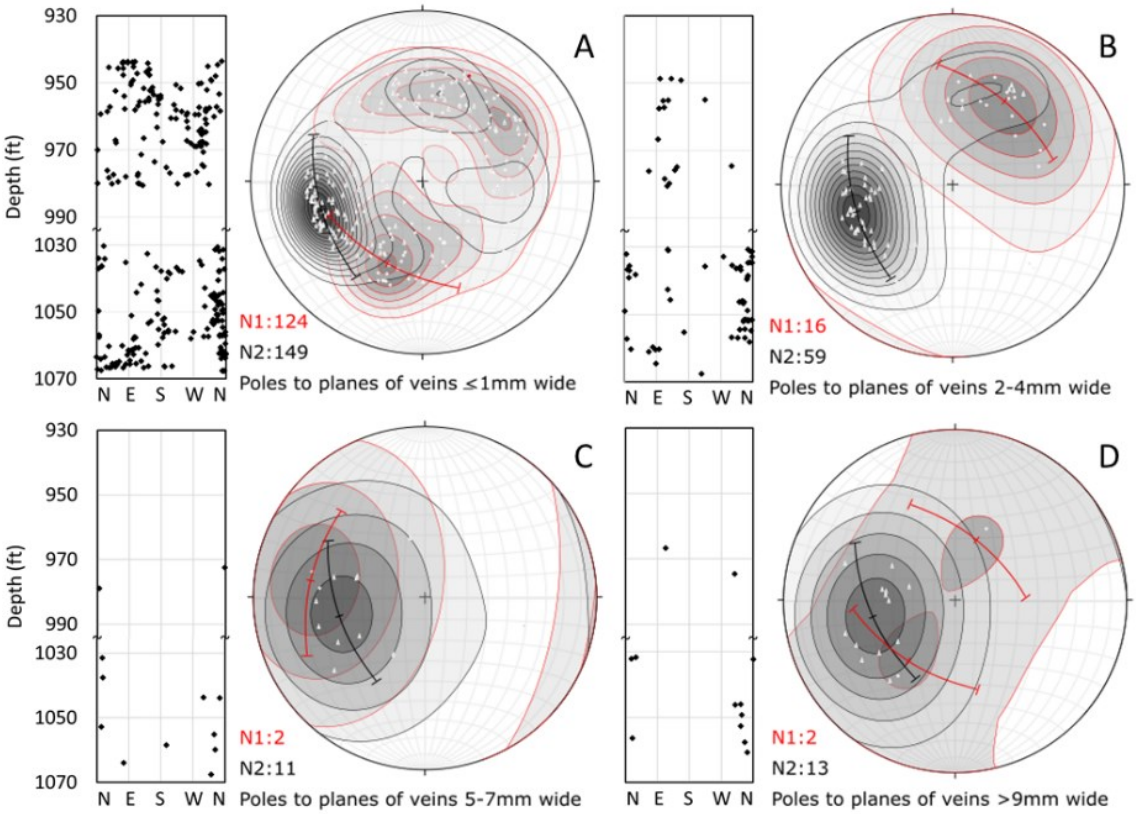

Figure 6: Stereonets of poles to planes for veins that A) are ≤1mm in, B) 2-4mm, C) 5-7mm, and D) >9mm in width. Measurements from the 942-983 ft. run are in red, N1; 1030-1066 ft. run are in black, N2. N indicates the number of measurements. Kamb contours have a significance level of 3 and an interval of 2. Error bars are ±30°. Note the scale break on depth verses strike plots.

4.2.3 Cross Cutting Relations

Veins that show clear cross cutting relationships between sets were rare. In the 942-983 ft. run SE trending veins and fractures tend to cross cut NW trending veins (Figure 7A, B). Around 1038 ft. depth there are N trending veins that are cross cut by veins and fractures of all orientations. Between 1050 and 1066 ft. depth there are predominantly ESE and NNW fractures and veins cross cutting veins of all trends (Figure 7A, B). Overall, we see that there are slightly more SE trending veins that are cross cutting than any other orientation (Figure 7B), whereas fractures and veins that have been offset range in strike, with concentrations in the SE and NNW (Figure 7A).

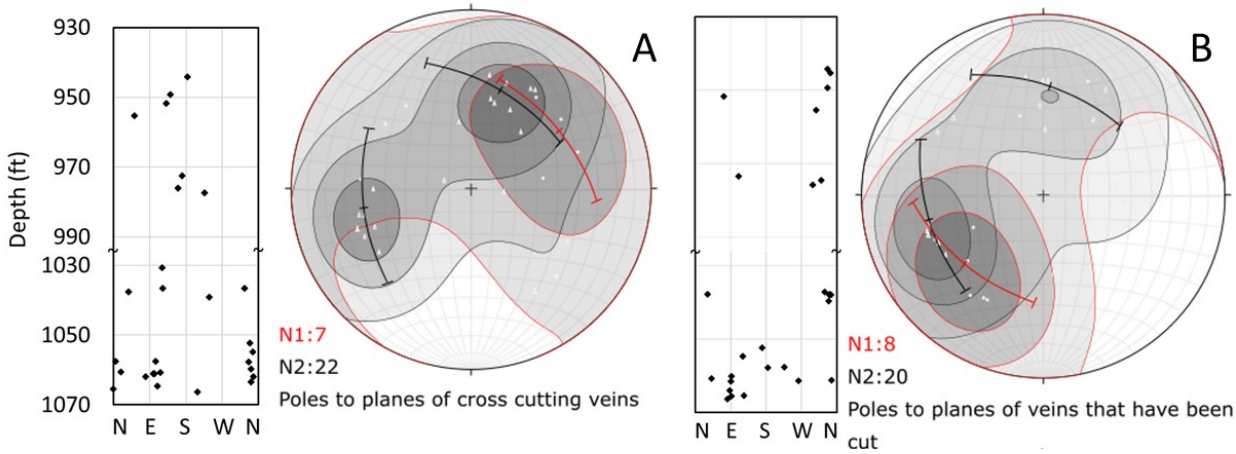

Figure 7: Stereonets of poles to planes for veins that A) are being cut by other veins and B) cross cutting other veins. Where veins were offset by more than a few millimeters a fracture or vein of the similar strike and dip was added to plot A to represent the offset feature that could not be measured. Measurements from the 942-983 ft. run are in red, N1; 1030-1066 ft. run are in black, N2. N indicates the number of measurements. N indicates the number of measurements. Kamb contours have a significance level of 3 and an interval of 2. Error bars are ±30°. Note the scale break on depth verses strike plots.

3.2.4 Veins with Slickenlines

Veins with slickenlines and veins that show dip slip extension are prevalent throughout all depths in both runs (Figure 8). Veins that have slickenlines with a rake between 80º-90º (Figure 8A, B) predominantly have strikes that trend E and N. In the 942-983ft. run the veins with high angle slikenlines range in strike from NE to SW, and in the 1030-1066ft. run they have strikes that are scattered between N to E. Veins that had slickenlines with rakes less than eighty degrees had an absolute average of 36º from horizontal (Figure 8C, D). These fractures are predominantly E-W striking in the 942-983ft. run and transition from SW striking to E striking with depth in the 1030-1066 ft. run. Furthermore, the direction of the slickenlines point to the E for the NW-SE striking veins, whereas the E striking veins contain slickenlines with lower angle rakes pointing to both the E and W (Figure 8D).

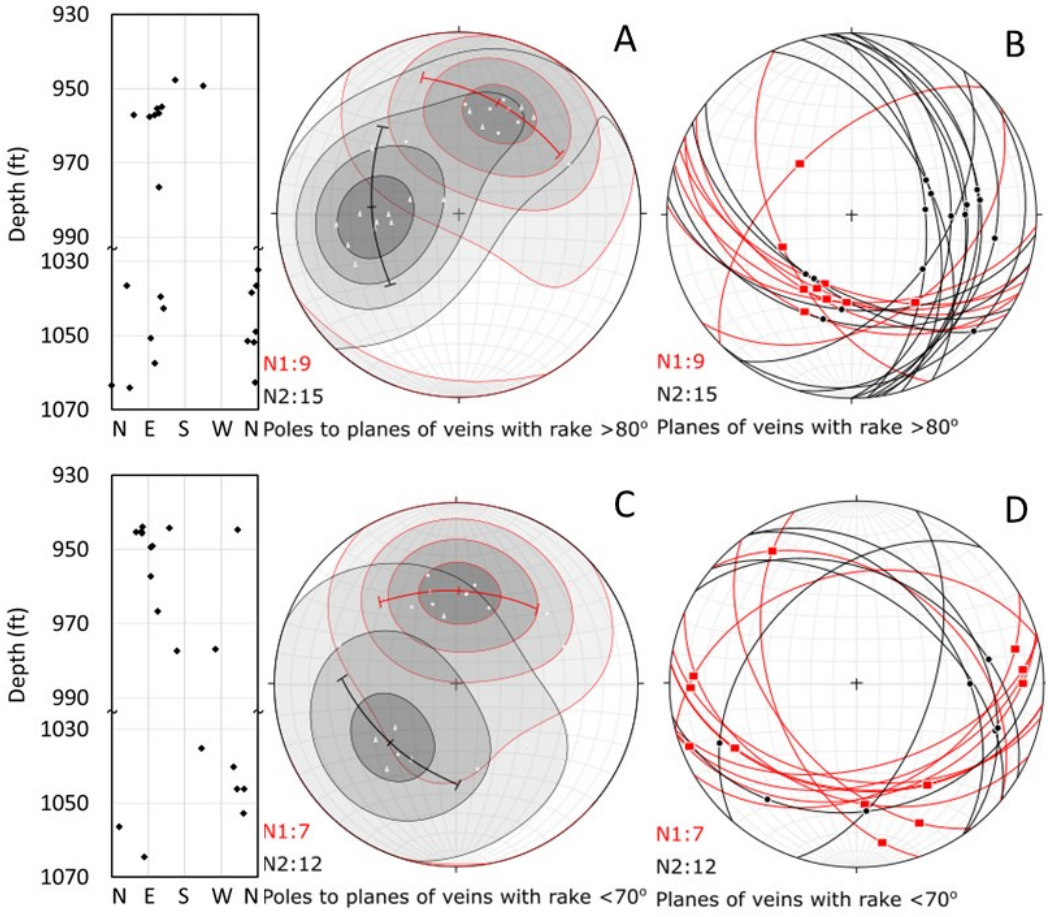

Figure 8: Stereonets of poles to planes for fractures with slikenline rakes A) >80º C) <70º. Stereonets of fracture planes (lines) with rake (dots) for fractures with slikenline rakes B) >80º and D) <70º. Veins that show dip slip extension are included in A and B. N indicates the number of measurements. Measurements from the 942-983 ft. run are in red, N1; 1030-1066 ft. run are in black, N2. N indicates the number of measurements. Kamb contours have a significance level of 3 and an interval of 2. Error bars are ±30º. Note the scale break on depth verses strike plots.

4. DISCUSSION

Non-mineralized fractures are interpreted to be a result of reduced overburden pressure caused by drilling because the fractures, on average, are horizontal. Mineralized veins are interpreted to indicate fluid flow, with thicker veins indicating prolonged fluid flow because minerals take time to grow. Laminated veins are interpreted to indicate episodic expansion because the laminated veins have multiple generations of mineral growth present. Furthermore, some laminated veins have mineralized cal that switches sides on the vein which indicates that the first generation of mineralization was ruptured during expansion. The laminated veins that show dip slip extension are indicators that the N, and SE trending vein sets have undergone sustained and episodic expansion. In addition, the thickest veins (Figure 6C, D), which indicate prolonged fluid flow are similarly striking to the N and dipping to the E. Conversely, the orientation of hairline veins (Figure 6A), which indicate a single event of fluid flow have orientations that are scattered in the 942-983 ft. run but concentrated in the NW in the 1030-1066 ft. run. Of the veins that are 2-4mm wide there is a SE-trending set that is consistent between both runs (Figure 6B). This could indicate that the SE-trending structures are important fluid pathways, but perhaps not as old as the N-trending structures which have been major fluid pathways for some time as evidenced by the large width and high density of veins along that strike.

The direction of slickenline rake in the low angle rake measurements indicates a down to the E oblique dextral slip on NW trending faults (Figure 8D). The E trending faults have very shallow slickenline rakes, which indicate a larger strike-slip component, both dextral and sinistral (Figure 8D). High angle slickenline rakes (Figure 8B) indicate dip-slip motion along SE-trending structures throughout both cores but N-trending structures only in the 1030-1066 ft. run. Cross cutting relations (Figure 7) in the 942-983 ft. run and in the upper 20 ft. of the 1030-1066 ft. run indicate that the N-trending, E-dipping vein set is older than the SE-trending, SW-dipping structures. However, in the lower half of the 1030-1066 ft. run there is a prominent NNW-striking set of veins that are cross-cutting veins of all orientation, which would mean these NNW-trending veins are younger, or at least the youngest structures in that depth range. These anomalously "young" veins coincide with the thickest veins at 1050-1066 ft. depth (Figure 6D) which otherwise show evidence of being very old, as discussed above. It could be that the N-trending, E-dipping fluid pathways are so well established that offsetting strain is redirected onto that N-trending plane rather than offsetting it, which would explain the bimodal orientation of dip-slip motion observed only in the 1030-1066 ft. run.

We propose that the N-trending, E-dipping structures are the older, more established fluid pathways and the SE-trending structure is the younger. Furthermore, we propose that the area has experience E-W to NE-SW extension which is accommodated as dip slip movement along N to NNW and SE trending structures, strike slip movement along E trending structures, and oblique down to the E movement along NW trending structures. These data support the hypothesis of Bergfeld et al., (2014) by documenting a strain environment at depth with matches observed extensional features produced by the seismic swarm of 1996. Additionally, we have shown that the SE-trending SW-dipping structures are likely younger and would dilate in the E-W to NE-SW extensional environment.

The hot springs that experienced an increase in discharge are aligned along a NE-trending, valley parallel trend. This is documented as a fault (Stelling et al., 2015), but the dip direction is unconstrained. The proposed NE-trending fault appears to be truncated by the SE-trending SW-dipping fault because the hot springs are only present to the north of the SE-trending fault (Figure 1C). It is tempting to suggest that the well-established N-trending vein set that is observed in the core is connected to this proposed NE-trending fault, particularly because the orientations are within error of each other and because the location of TG-4 is along strike with this permeable structure. In which case the dip direction would be to the SE parallel to the valley wall.

5. CONCLUSIONS

Core segments from well TG-4 in the Akutan geothermal resource area were reoriented using the declination of remanent magnetization and core logs created from photogrammetry techniques. Veins sets were defined based on orientation, minerology, width, slickenline rake, and crosscutting relations. The orientations of the hairline veins indicate that single flow events occur in many directions. However, the rupturing events that caused thick and or laminated veins occur more often along NNW-striking and ENE-dipping structures. More data is needed to confidently establish relative ages between vein sets, but overall the NNW-trending set is the older, better established pathway and the SE to E trending set is the younger, with lower amounts of mineralization. Slickenline rake data indicate ENE-WSW extension, which lends support to the hypothesis proposed by Bergfeld et al., (2014) that dilation along SE-trending faults have provided a pathway for fluid flow to daylight at hot springs in the eastern arm of Hot springs Bay Valley. Furthermore, we expand upon the work of Stelling et al. (2015) and propose that the prominent N-trending vein sets observed in the core could be connected to a proposed fault which is defined by the NE-trending linearity of hot springs. If this is correct the fault has a dip to the SE and is truncated by a younger SE-trending fault which likely ruptured during the 1996 seismic swarm.

6. AKNOWLAGMENTS

This work was supported by the Alaska Geological Society, the Geological Society of America, and the Western Washington Foundation. We thankfully acknowledge the work of Daniel Fragerlie in writing a python code that created masks of images for the photogrammetry process. Drilling was a collaboration between the City of Akutan and Geothermal Resource Group.

REFERENCES

Allerton, S.A., McNeill, A.W., Stokking, L.B., Pariso, J.E., Tartarotti, P., Marton, F.C., and Pertsev, N.N.: Structures and magnetic fabrics from the lower sheeted dike complex of Hole 504B reoriented using stable magnetic remanence, *in Proceedings of the Ocean Drilling Program, Scientific Results*, **137**, (1995), 245–251.

Bergfeld, D., Lewicki, J.L., Evans, W.C., Hunt, A.G., Revesz, K., and Huebner, M.: Geochemical investigation of the hydrothermal system on Akutan Islan, Alaska, July 2012, U.S. *Geological Survey Scientific Investigations Report Scientific Investigations Report.* (2014).

Byers, F.M., and Barth, T.F.W.: Volcanic activity on Akun and Akutan islands, *Proceedings Seventh Pacific Sciense Congress*, **2**, (1953)

Finch, R.H.: Akutan volcano, *Volcanological Review*, **16**, (1935), 155–160.

Fisher Ronald Aylmer: Dispersion on a sphere, *Proceedings of the Royal Society of London. Series A. Mathematical and Physical Sciences*, **217**, (1953), 295–305.

Fuller, M.: Magnetic orientation of borehole cores, *Geophysics*, **34**, (1969), 772–774.

Hailwood, E.A., and Ding, F.: Palaeomagnetic reorientation of cores and the magnetic fabric of hydrocarbon reservoir sands, *Geological Society, London, Special Publications,* **98**, (1995), 245–258.

Kirschvink, J.L.: The least-squares line and plane and the analysis of palaeomagnetic data, *Geophysical Journal International,* **62**, (1980), 699–718.

Kolker, A., Bailey, A., and Howard, W.: The 2010 Akutan Exploratory Drilling Program: Preliminary Findings, *Geothermal Resource Council Transactions,* **35**, (2011), 847–852.

Kolker, A., Stelling, P., Cumming, W., and Rohrs, D.: Exploration of the Akutan geothermal resource area, *in Proceedings, Thirty-Seventh Workshop on Geothermal Reservoir Engineering,* **37**, (2012).

Lu, Z., Wicks Jr, C., Kwoun, O., Power, J.A., and Dzurisin, D.: Surface deformation associated with the March 1996 earthquake swarm at Akutan Island, Alaska, revealed by C-band ERS and L-band JERS radar interferometry, *Canadian Journal of Remote Sensing,* **31**, (2005), 7–20.

Lurcock, P.C., and Wilson, G.S.: PuffinPlot: A versatile, user-friendly program for paleomagnetic analysis, *Geochemistry, Geophysics, Geosystems*, **13**, (2012).

Miller, T.P., McGimsey, R.G., Richter, D.H., Riehle, J.R., Nye, C.J., Yount, M.E., and Dumoulin, J.A.: Catalog of the historically active volcanoes of Alaska, *US Geological Survey Open-File Report*, **98**, (1998), 582.

Motyka, R.J., Liss, S.A., Nye, C.J., and Moorman, M.A.: Geothermal resources of the Aleutian arc, *Division of Geological and Geophysical Surveys*, (1993).

Motyka, R.J., and Nye, C.J.: A geological, geochemical, and geophysical survey of the geothermal resources at Hot Springs Bay valley, Akutan Island, Alaska, *Alaska Division of Geological & Geophysical Surveys Report of Investigations,* **88–3**, (1988), 115.

Pinto, M.J., and McWilliams, M.: Drilling-induced isothermal remanent magnetization, *Geophysics*, **55**, (1990), 111–115.

Romick, J.D., Perfit, M.R., Swanson, S.E., and Shuster, R.D.: Magmatism in the eastern Aleutian arc: temporal characteristic of igneous activity on Akutan Island, *Contributions to Mineralogy and Petrology*, **104**, (1990), 700–721.

Stelling, P., Hinz, N.H., Kolker, A., and Ohren, M.: Exploration of the Hot Springs Bay Valley (HSBV) geothermal resource area, Akutan, Alaska, *Geothermics*, **57**, (2015), 127–144.